Local- and intermediate-range partial structure study of As–Se glasses

Shinya Hosokawa[1*], Jens Rüdiger Stellhorn[2], Nathalie Boudet[3], Nils Blanc[3], Eisuke Magome[4], László Pusztai[5,6], Shinji Kohara[7], Kazutaka Ikeda[8], and Toshiya Otomo[9]

[1]*Institute of Industrial Nanomaterials, Kumamoto University, Kumamoto 860-8555, Japan*

[2]*Department of Physics, Nagoya University, Nagoya 464-8602, Japan*

[3]*Universitité Grenoble Alpes, CNRS, Grenoble INP, Institut Néel, 38000 Grenoble Cedex 9, France*

[4]*Kyushu Synchrotron Light Research Center, Tosu 841-0005, Japan*

[5]*Wigner Research Centre for Physics, 1525 Budapest, Hungary*

[6]*International Research Organization for Advanced Science and Technology (IROAST), Kumamoto University, Kumamoto 860-8555, Japan*

[7]*National Institute for Materials Science (NIMS), Tsukuba 305-0047, Japan*

[8]*Neutron Industrial Application Promotion Center, Comprehensive Research Organization for Science and Society (CROSS), Tokai 319-1106 Japan*

[9]*Institute of Materials Structure Science, High Energy Accelerator Research Organization (KEK), Tsukuba 305-0801, Japan*

To investigate the relationship between the partial structures and the stiffness transition in As_xSe_{1-x} glasses, anomalous X-ray scattering (AXS) and X-ray and neutron diffraction (XRD and ND) experiments were carried out. For the AXS experiments, anomalous terms near the absorption edges were experimentally obtained instead of the theoretical values with large ambiguities. The results were analyzed by reverse Monte Carlo (RMC) modeling to obtain partial structure factors, $S_{ij}(Q)$, partial pair distribution functions, $g_{ij}(r)$, and three-dimensional atomic configurations. The $S_{ij}(Q)$ and $g_{ij}(r)$ functions gradually vary with x; however, an important change was observed in the intermediate-range element-selective atomic structures (the so-called hyper-ordered structures) near the stiffness transition composition. With decreasing x across the so-called intermediate phase compositions, a rapid decrease of the As–As wrong bonds is visualized. However, the other anomalies found in Ge–Se glasses are not clearly observed, such as a rapid decrease in pre-shoulder position in $S_{\mathrm{SeSe}}(Q)$, a rapid decrease in the number of edge-sharing connections, and an exclusion tendency of the connections between the As(Ge) atoms sharing two Se atoms, which may be related to the anisotropic pyramidal atomic configurations around the As atoms in the As-Se glasses in contrast to the isotropic tetrahedral ones around the Ge atoms in the Ge-Se glasses.

1. Introduction

A mean-field theory[1,2] is a simple idea for understanding various experimental anomalies around a specific composition of the rigidity percolation threshold at the average coordination number $\langle r \rangle = 2.4$, where the number of configurational constraints per atom is equal to the degrees of freedom in three dimensions. The character of a network glass undergoes a transition from rigid at $\langle r \rangle > 2.4$ to easily deformable (floppy) at $\langle r \rangle < 2.4$. In the case of the As_xSe_{1-x} glasses handled in this paper, the threshold composition corresponds to $x = 0.40$, the As_2Se_3 stoichiometric alloy, if the coordination numbers of the As and Se atoms are exactly 3 and 2, respectively. At the beginning of more than 15 years of researches, the findings were limited to the relationship between the rigidity percolation and physical properties of binary[3,4] and ternary[5,6] chalcogenide glasses and liquids.

Remarkable experimental progress concerning the stiffness transition has been achieved by Boolchand and coworkers on Ge_xSe_{1-x} glasses.[7,8] They demonstrated that the results of Raman scattering, modulated scanning calorimetry (MDSC), and Mössbauer spectroscopy on a fine composition grid provide evidence that the transition occurs over a well-defined

*Corresponding author: shhosokawa@kumamoto-u.ac.jp

composition range between an onset point at $\langle r \rangle = 2.40$ ($x = 0.20$) and a composition point at $\langle r \rangle = 2.52$ ($x = 0.26$), where the glasses are characterized to be in an unstressed-rigid region called an *intermediate phase* (IP).

To explore the relationship between atomic structures in short and intermediate ranges in Ge_xSe_{1-x} glasses, Hosokawa et al. carried out anomalous X-ray scattering (AXS) and neutron diffraction (ND) experiments, and analyzed the obtained experimental data by reverse Monte Carlo (RMC) modeling to obtain partial structure factors, $S_{ij}(Q)$, partial pair distribution functions, $g_{ij}(r)$, and the corresponding three-dimensional (3D) atomic configurations.[9,10] From these experiments, important indications of the stiffness transition were observed on the basis of the intermediate-range element-selective atomic structures (*hyper-ordered structures*). Namely, a sudden decrease in prepeak intensity in $S_{\mathrm{GeGe}}(Q)$, an abrupt disappearance of Ge–Ge wrong bonds, anomalies in the connection ratio of edge- and corner-sharing $GeSe_4$ tetrahedra, and a characteristic change in the features of tetrahedral connections were realized with decreasing x across the IP concentration range. During the analytical process, we confirmed that AXS is sufficiently sensitive to obtain intermediate-range structures,[9] while ND has an excellent capability to correctly determine the nearest neighboring structures.[10]

Concerning the As–Se glasses handled in this study, Georgiev et al.[11] carried out a MDSC experiment on As_xSe_{1-x} glasses and determined the IP region between $\langle r \rangle = 2.29$ and 2.37 ($x = 0.29$ and 0.37, respectively). Two differences are seen in the features of the IP. The first one is that the x range of IP is a wide value of 0.08 compared with 0.06 for Ge_xSe_{1-x} glasses. In the sense of $\langle r \rangle$, however, the As_xSe_{1-x} glasses have a smaller $\Delta\langle r \rangle$ of 0.08 than 0.12 for the Ge_xSe_{1-x} glasses. The second one is that the IP range shifts to the smaller $\langle r \rangle$ values from the original value of 2.40 in the As_xSe_{1-x} glasses but toward the opposite direction in the Ge_xSe_{1-x} glasses. For this reason, Georgiev et al.[11] predicted the existence of fourfold-coordinated quasi-tetrahedral Se=$AsSe_3$ configurations instead of threefold-coordinated $AsSe_3$ pyramids by about 30% in number to increase the $\langle r \rangle$ values. This results in breaking the "$8-N$ bonding (octet) rule" that is usually accepted for network glasses.

The above idea motivated experimental studies of partial structures, and Hosokawa et al.[12] carried out AXS experiments on As_2Se_3 in combination with RMC modeling to examine whether the $8 - N$ bonding rule is broken around the As atoms or not. Note that ND with isotope substitution (NDIS) experiments is usually very effective for obtaining partial structures. Since As has only one stable ^{75}As isotope, however, this technique is limited to the use of Se isotopes. In fact, recent NDIS studies of As_xSe_{1-x} glasses at $x = 0.40$, 0.35, and 0.30 by Polidori et al.[13] result in only difference functions around the As and Se elements. An *ab*

initio molecular dynamics (MD) simulation was also conducted to confirm the experimental results. The results are rather ambiguous, i.e., the experimental AXS gave the coordination number around As, N_{As}, of 3.26(2), which is in good agreement with Georgiev et al.'s prediction, while the theoretical data resulted in $N_{\mathrm{As}} = 3.07(3)$, which could not confirm the validity of the experimental results.

Subsequent AXS experiments were carried out also in the IP region.[14] The obtained N_{As} values were 3.29 and 3.69 at $x = 0.33$ and 0.29, respectively, showing good coincidence at $x = 0.33$ but apparent overestimation at $x = 0.29$. In addition, the spectral changes in the $S_{\mathrm{AsAs}}(Q)$ partials were not systematic, particularly on the first peaks at about $Q = 20$ nm^{-1}.

To investigate the relationship between the local- and intermediate-range atomic structures and the stiffness transition in $\mathrm{As}_x\mathrm{Se}_{1-x}$ glasses, four technical improvements that enable more systematical and reliable structural data than the above previous results to be obtained were achieved in the present study. 1) Experiments were performed in a wide range of $0.20 \leq x \leq 0.40$ including the floppy, unstressed-rigid (IP), and rigid regions. 2) As K AXS measurements were conducted using a new setup at Kyushu Synchrotron Light Research Center (Saga-LS). 3) Experimental anomalous terms of atomic form factors were obtained and used for the analysis. 4) ND data were introduced to obtain more accurate first-neighboring information. As a result, different conclusions were obtained for the N_{As} values from those in the previous papers.

In this article, we explain the experimental technique in Sec. 2, present full sets of $S_{ij}(Q)$s, $g_{ij}(r)$s, and the 3D atomic configurations in Sec. 3, and discuss the specific features of the glass structures, such as prepeak heights and positions, partial coordination numbers, and connections of AsSe_3 pyramids, in relation to the stiffness transition or IP compositions in Sec. 4. Finally, we summarize the present results in Sec. 5.

2. Experimental and analytical procedures

Bulk $\mathrm{As}_x\mathrm{Se}_{1-x}$ glass samples with $x = 0.20$, 0.25, 0.29, 0.33, 0.37, and 0.40 were prepared by quenching the melts in silica ampoules containing proper compositions of As and Se with purities of 99.999 at.%. The melts were homogenized at 600°C for at least 48 h with the frequent stirring of the ampoule and quenched in air. The temperature was chosen by taking the boiling point of As element at about 613°C and of Se at about 685°C into account.

AXS measurements near the As K absorption edge (11.868 keV) were carried out at BL15 of the Saga-LS at Tosu, Japan. The voltage and current of this ring are 1.7 GeV and 100–300 mA, respectively. To compensate relatively weak X-ray intensities from such a small

synchrotron ring, we used two Si drift detectors (SDDs) to sensitively detect the elastic scattering X-rays and correctly estimate fluorescent X-ray contributions in the detected scattering signals. The elastic scattering signals reach 0.6–0.8 million counts at the $S(Q)$ maximum in a reasonable beamtime at Saga-LS; these are sufficient for the analysis to obtain differential structure factors, $\Delta_k S(Q)$. The details of this AXS detecting system are given elsewhere.[15)]

AXS experiments near the Se K edge (12.658 keV) were performed at BM02 of the European Synchrotron Radiation Facility (ESRF) at Grenoble, France. To obtain sufficient elastic signals and exclude the fluorescent X-rays, we used a bent graphite crystal analyzer and a scintillation counter on a 1-m-long arm. The details of this detecting system are given in Ref. 9 and in a review article.[16)] Both the AXS experiments were carried out in reflection mode for rectangle samples with a width of about 5 mm, a length of about 10 mm, and a thickness of about 2 mm flattened with an emery paper.

The improvement of these AXS experiments is made to enable us to experimentally determine anomalous terms of atomic form factors near an absorption edge. For this, X-ray absorption spectra, μ, were measured in the fluorescence mode near an absorption edge of the k element. The energy ranges for the absorption measurements were about 11.8-12.0 and 12.6-12.8 keV for the As and Se edges, respectively. The obtained μ spectra were smoothly connected with the imaginary part f'' of the anomalous term, since μ is proportional to f'' and is expressed as

$$\mu = -2\lambda r_e \sum_i n_i f_i'',$$

where λ is the wavelength of X-rays, r_e is the classical electron radius, and n_i is the number of electrons in the ith element. For this, Sasaki's theoretical data[17)] were used for f'' outside the measured E range. The upper three spectra of Fig. 1 show the f'' spectra near the (a) As and (b) Se K absorption edges at selected x values of 0.20, 0.29, and 0.40. As seen in the panels, the f'' spectra as well as those at other x values are mostly independent of x.

The real part f' of the anomalous term can be calculated using the Krammars–Kronig relation

$$f'(E) = \frac{2}{\pi} \mathrm{P} \int_0^\infty \frac{E' f''(E')}{E'^2 - E^2} \mathrm{d}E',$$

where P denotes the principal value. The results are given in the lower spectra in Fig. 1. As seen in the figures, the f' spectra are mostly independent of x.

The dashed lines in Fig. 1 indicate the energy positions at 20 and 200 eV below the corresponding K absorption edges where the present AXS measurements were carried out

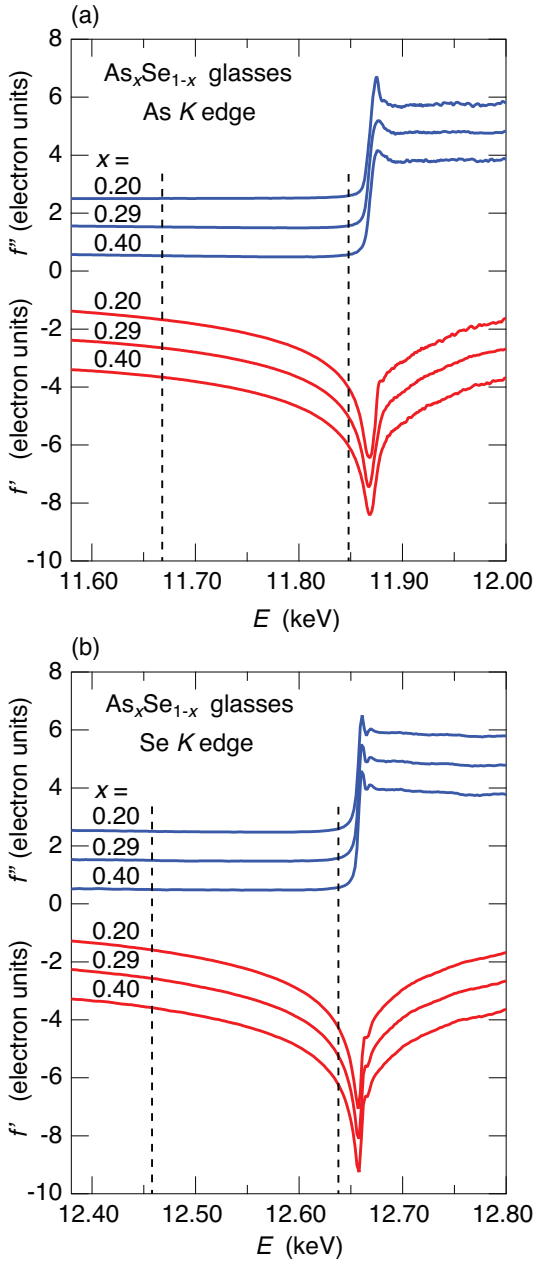

Fig. 1. Experimental anomalous terms f' (real) and f" (imaginary) near the (a) As and (b) Se K absorption edges of selected As_xSe_{1-x} glasses. For clarity, the correct curves are at $x = 0.40$ and others are displaced upward by 1. Dashed lines indicate the energy positions at 20 and 200 eV below the corresponding edges where the present AXS measurements were carried out. (Color online)

(E_{near} and E_{far}, respectively). Since the f' and f'' values at six compositions are almost the same, we employed the average values in the following data analyses, as tabulated in Table I. The errors were estimated to be 0.02 for f' at E_{near} and 0.01 for other values. For clarity, the correct curves are at $x = 0.40$ and others are displaced upward by 1.

Table I. Experimentally obtained f' and f'' values of As and Se in electron units at energies measured and the theoretical values[17] in parentheses.

Element	E (keV)	f'_{As}	f''_{As}	f'_{Se}	f''_{Se}
As	11.668	–3.673	0.507		
		(–3.704)	(0.512)	(–2.241)	(0.580)
	11.848	**–6.039**	0.602		
		(–6.054)	(0.497)	(–2.419)	(0.564)
Se	12.458			–3.627	0.497
		(–2.236)	(3.494)	(–3.739)	(0.514)
	12.638			**–5.683**	0.532
		(–1.960)	(3.413)	(–5.625)	(0.501)

In Table I, values in parentheses indicate the theoretical results calculated by Sasaki.[17] The differences in f' obtained in the present experiments are larger than theoretical values by about 0.7 and 9.0% near the As and Se edges, respectively, which may affect the validity of the coordination numbers. In the previous AXS experiments on Ge_xSe_{1-x} glasses,[9] where E_{near} was selected at the nearer energy of 15 eV below the corresponding K edges, corrections from theoretical f' and f'' values were achieved by comparing the $S_{ij}(Q)$ data of $GeSe_2$ obtained from AXS results with reliable NDIS results obtained by Petri et al.,[18] and the differences of about 14 and 3% were estimated for f' of Ge and Se, respectively. Hence, to determine local glass structures, it is important to experimentally obtain f' and f'' values. For the following analysis, theoretical values are used at energies where the experimental values are missing.

To obtain element-selective structural information, one can obtain the differences between two scattering data values at E_{near} and E_{far}. The differential structure factors, $\Delta_k S(Q)$, can be related to the differential intensity, $\Delta_k I$, as

$$\alpha_k \Delta_k I(Q, E_{far}, E_{near}) = \Delta_k[\langle f^2 \rangle - \langle f \rangle^2] + \Delta_k[\langle f \rangle^2] \Delta_k S(Q),$$

where α_k is a normalization constant and $\Delta_k[\ ]$ indicates the difference between the values in brackets at E_{far} and E_{near} close to an absorption edge of the kth element.

The $\Delta_k S(Q)$ functions are separated into three $S_{ij}(Q)$s as

$$\Delta_k S(Q) = \sum_{i=\mathrm{As,Se}} \sum_{j=\mathrm{As,Se}} W_{ij}^k S_{ij}(Q),$$

where the weighting factors, W_{ij}^k, are given by

$$W_{ij}^k(Q, E_{far}, E_{near}) = x_i x_j \frac{\Delta_k[f_i f_j]}{\Delta_k[\langle f \rangle^2]},$$

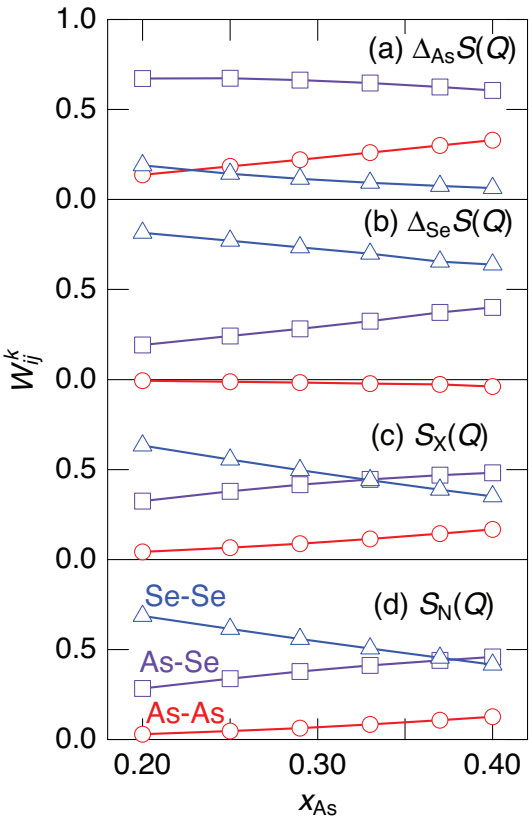

Fig. 2. W_{ij}^k values of As–As (◯), As–Se (□), and Se–Se (△) correlations for As_xSe_{1-x} glasses as a function of x for (a) $\Delta_{As}S(Q)$, (b) $\Delta_{Se}S(Q)$, (c) $S_X(Q)$, and (d) $S_N(Q)$. W_{ij}^k values for X-ray data are shown at $Q = 22$ nm^{-1} near the first maximum of $S_X(Q)$. (Color online)

The W_{ij}^k values were calculated by using the f' and f'' values together with theoretical values of the usual energy-independent term, $f_0(Q)$, taken from the literature.[19)]

Circles, squares, and triangles in Fig. 2 show the W_{ij}^k values of the As–As, As–Se, and Se–Se correlations, respectively, as a function of x for (a) $\Delta_{As}S(Q)$, (b) $\Delta_{Se}S(Q)$, and (c) total X-ray structure factors, $S_X(Q)$, at $Q = 22$ nm^{-1} near the first maximum of $S_X(Q)$. They all vary slightly with Q. Since W_{AsSe}^k and W_{SeAs}^k are the same as easily understood by the definition, and the twice of W_{AsSe}^k is generally used as the weighting factor of $S_{AsSe}(Q)$. According to such a common practice, twice the values are drawn for W_{AsSe}^k in Fig. 2. As expected from the principle of AXS, the As–As and Se–Se contributions are highly suppressed in $\Delta_{Se}S(Q)$ and $\Delta_{As}S(Q)$, respectively. Concerning the As composition x, the As–As contribution terms increase with x, while the Se–Se terms decrease. The As–Se terms change with x, depending on the respective structure factors.

ND measurements were carried out over a wide Q range from 1.6 to more than 1000 nm^{-1}, using the neutron total scattering spectrometer (NOVA)[20)] installed at BL21 of the Material

and Life Experimental Facility (MLF) of the Japan Proton Accelerator Research Complex (J-PARC), Tokai, Japan. The incident neutron beam was generated by the proton accelerator with an output power of 400 kW. Measurements were performed in the time-of-flight mode, with neutron energies between 0.0013 and 5.7 eV, and a pulse repetition rate of 25 Hz. Details of the neutron detecting system are given elsewhere.[10)]

The same glassy samples of about $5\times10\times2$ mm^3 were also used for the ND measurements to measure the structures with the same compositional and thermal conditions. The samples were contained in standard pure V sample containers with an outer diameter of 10.0 mm and a thickness of 0.1 mm. Experiments took 4 h each. Detected ND intensities from the samples were corrected for instrumental background, absorption by samples and cells,[21)] and multiple[22)] and incoherent scattering. The scattering lengths and absorption cross-sections for the constituent nuclei were taken from the literature.[23)] These corrections were carried out with the mvaSq program coded by the NOVA group.[24)]

The W_{ij}^{k} values for total neutron structure factors, $S_{\mathrm{N}}(Q)$, obtained from ND experiments are shown in Fig. 2(d); they were calculated from scattering lengths, b_i, of 6.58 fm for As and 7.970 fm for Se,[23)] instead of f for the X-ray data. b_{Se} is larger than b_{As} by 21%, while f_{Se} exceeds f_{As} by only about 3%. Thus, W_{SeSe} values for $S_{\mathrm{N}}(Q)$ are slightly larger than those for $S_{\mathrm{X}}(Q)$, whereas the others are the opposite.

RMC modeling[25,26)] was applied to obtain atomic configurations from the present experimental data of two $\Delta_k S(Q)$s, $S_{\mathrm{X}}(Q)$, $S_{\mathrm{N}}(Q)$, and the corresponding neutron total pair distribution functions, $g_{\mathrm{N}}(r)$. Calculation cubic boxes contained 10,000 atoms in total with edge lengths determined using density data.[27)] Initial atomic configurations were generated by hard-sphere Monte Carlo simulations. Three constraints were applied to the RMC calculations: 1) shortest atomic distance of 0.220 nm, 2) weak $8-N$ connectivities, and 3) weak bond angle constraint of 100° around As atoms. RMC simulations were carried out using the RMC++ program package.[28)]

3. Results

The circles in Fig. 3 show experimental results of (a) $\Delta_{\mathrm{As}}S(Q)$, (b) $\Delta_{\mathrm{Se}}S(Q)$, (c) $S_{\mathrm{X}}(Q)$, (d) $S_{\mathrm{N}}(Q)$, and (e) $g_{\mathrm{N}}(r)$ of $\mathrm{As}_x\mathrm{Se}_{1-x}$ glasses. The $S_{\mathrm{X}}(Q)$ results seem to be consistent with the pioneering XRD data obtained in 1973 by Renninger and Averbach,[29)] and the $S_{\mathrm{N}}(Q)$ and $g_{\mathrm{N}}(r)$ results are in good agreement with those of a recent ND work with natural isotopic abundances by Polidori et al.[13)] All of the spectra gradually vary with changing x, and seem to have no characteristic features in the structures across the IP region of $x = 0.29 - 0.37$.

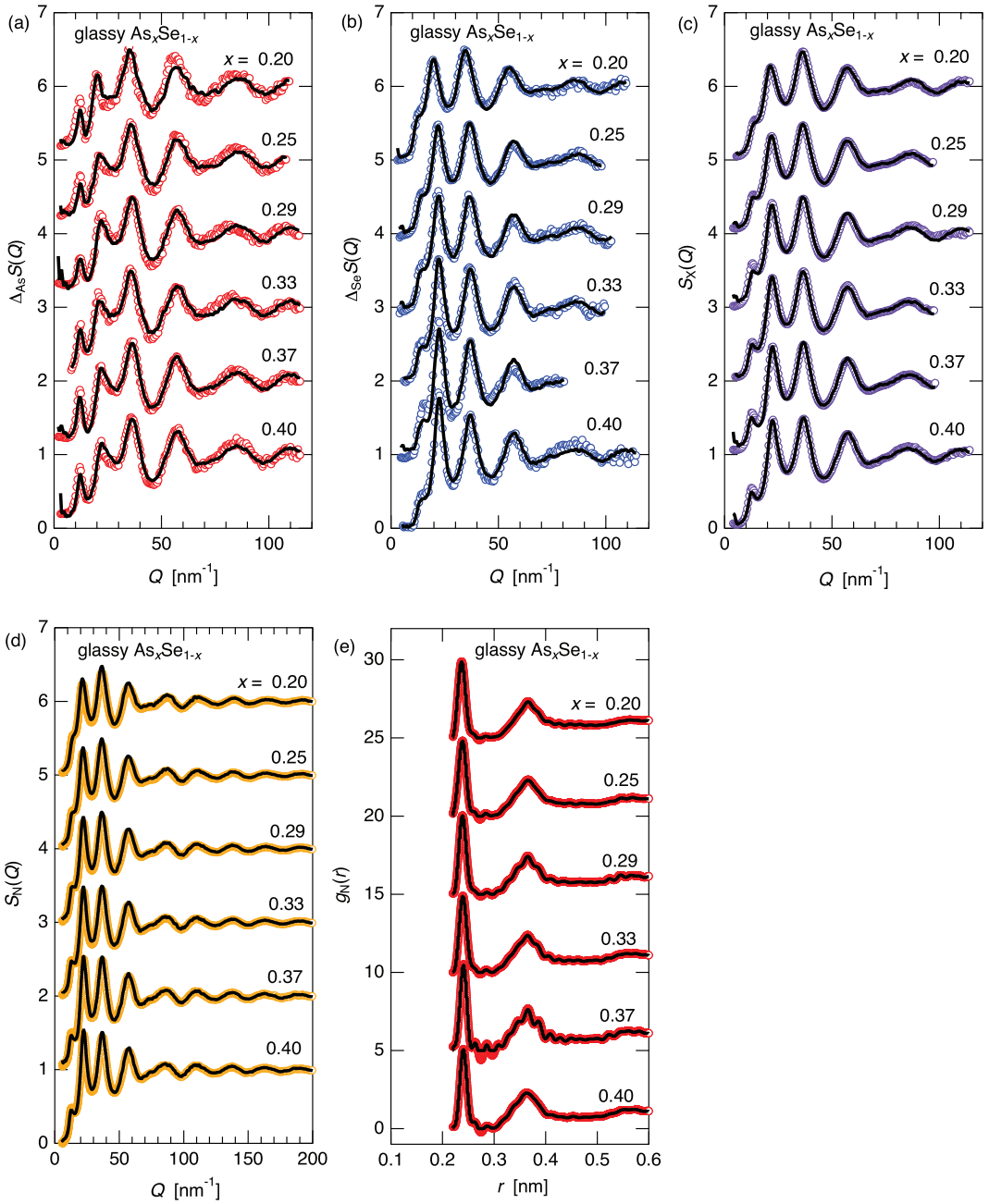

Fig. 3. Circles indicate experimental results of (a) $\Delta_{As}S(Q)$, (b) $\Delta_{Se}S(Q)$, (c) $S_X(Q)$, (d) $S_N(Q)$, and (e) $g_N(r)$ of As_xSe_{1-x} glasses. Solid curves represent the best fits of RMC modeling. For clarity, the data are displaced upward by 1 for (a)–(d) and 5 for (e). (Color online)

The spectral features of structural factors with different W_{ij}^k values are very different from each other; $\Delta_{As}S(Q)$s have large and sharp prepeaks at about $Q = 12$ nm^{-1}, and small first peaks at about 20 nm^{-1}. On the other hand, $\Delta_{Se}S(Q)$s exhibit only shoulders at the larger Q value of about 15 nm^{-1} and large first peaks. Both the $S_X(Q)$ and $S_N(Q)$ spectra show intermediate features between those of $\Delta_{As}S(Q)$s and $\Delta_{Se}S(Q)$s. The $S_X(Q)$ and $S_N(Q)$ spec-

tra look similar; however, the prepeaks in $S_X(Q)$s are slightly more prominent than those in $S_N(Q)$s. These differences are, of course, due to the differences in W_{ij}^k given in Fig. 2. When the Q values exceed 30 nm^{-1}, all the spectra in Figs. 3(a)–(d) look very similar to each other. The $g_N(r)$ functions in Fig. 3(e) have prominent peaks at about 0.23 nm and a second peak at about 0.37 nm.

The solid curves in Fig. 3 indicate the RMC fits for the corresponding spectra. Although the coincidences between the results of experiments and the RMC fits are very good, small inconsistencies between the experimental data and the RMC fits are seen in the AXS data of $\Delta_k S(Q)$ in Figs. 3(a) and (b). This is because the contrasts in the AXS data are only several percent of the scattering data of $S_X(Q)$s. With decreasing x, the prepeak heights in $\Delta_{As}S(Q)$s do not show systematic changes with x, while the shoulders in $\Delta_{Se}S(Q)$s at about 15 nm^{-1} seem to slowly rise. The prepeaks or shoulders in $S_X(Q)$s and $S_N(Q)$s become broadened. The heights of prominent peaks in $g_N(r)$s become alightly lower, indicating that the As–Se and Se–Se bond lengths are almost identical, and the average coordination numbers decrease with decreasing x.

Figure 4 shows (a) $S_{AsAs}(Q)$, (b) $S_{AsSe}(Q)$, and (c) $S_{SeSe}(Q)$ partial structure factors of As_xSe_{1-x} glasses obtained by the present RMC modeling. For the stoichiometric $As_{0.40}Se_{0.60}$ glass, a sharp peak is observed at the prepeak position of total structures of about 12 nm^{-1} shown in Figs. 3(c) and (d). The first peak of $S_{AsAs}(Q)$ is clearly observed at about 20 nm^{-1}, which is different from the previous AXS reports,[12,14] but looks reasonable upon comparison with those at different x values. This would be a result of adding the ND data to the present RMC analysis. The $S_{AsSe}(Q)$ spectrum also has a prepeak at a similar position in $S_{AsAs}(Q)$. A sharp minimum is seen at about 18 nm^{-1}, which is a slightly lower Q position than the first peak position in $S_X(Q)$ and $S_N(Q)$ of about 22 nm^{-1}. A small shoulder is observed at the sharp first peak in $S_X(Q)$ and $S_N(Q)$. Beyond 30 nm^{-1}, the spectral features are similar to those in $S_N(Q)$, indicating that the As–Se bonding is the main contribution in $As_{0.40}Se_{0.60}$ glass. The $S_{SeSe}(Q)$ spectrum has a shoulder (not a peak) at about 15 nm^{-1}, a sharp and large first peak at about 22 nm^{-1}, and a second peak at about 37 nm^{-1} (similar features to $S_X(Q)$ and $S_N(Q)$). These features were also observed for the $GeSe_2$ glasses.[9,10]

With decreasing x, all of the $S_{ij}(Q)$ spectra gradually change. The prepeak in $S_{AsAs}(Q)$ exists over the entire x range measured, while the prepeak height does not change systematically with x. The first peak in $S_{AsAs}(Q)$ does not change distinctly but looks not to be systematic. The $S_{AsAs}(Q)$ spectrum remains unchanged approximately beyond 30 nm^{-1}, and the errors become more conspicuous with decreasing x. These unstable spectral features in

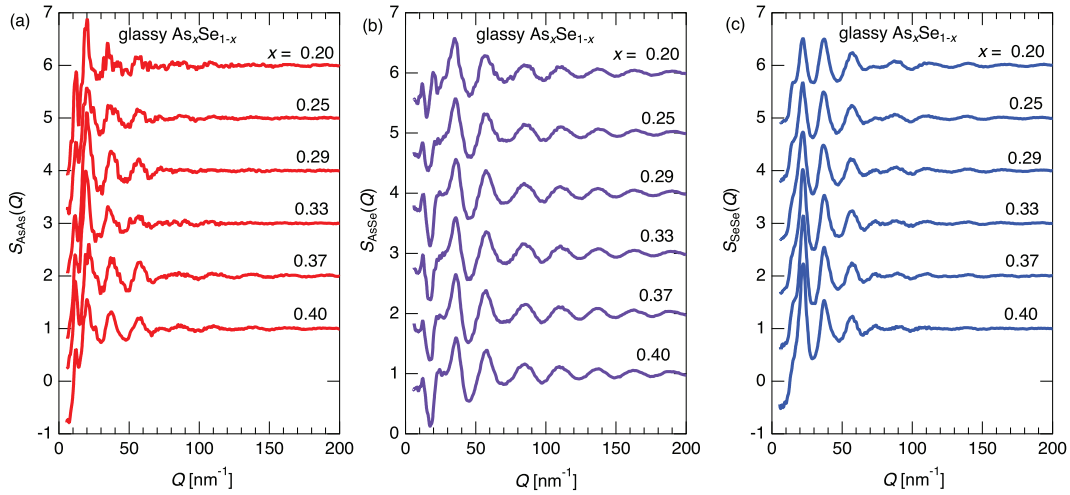

Fig. 4. (a) $S_{\mathrm{AsAs}}(Q)$, (b) $S_{\mathrm{AsSe}}(Q)$, and (c) $S_{\mathrm{SeSe}}(Q)$ of As_xSe_{1-x} glasses obtained by the present RMC modeling. For clarity, the data are displaced upward by 1. (Color online)

the As–As correlations are due to the small W^k_{AsAs} values even for the $\Delta_{\mathrm{As}}S(Q)$ data shown in Fig. 2. The prepeak in $S_{\mathrm{AsSe}}(Q)$ remains unchanged, while the minimum at about 18 nm^{-1} is highly buried with decreasing x. The remaining spectra beyond 30 nm^{-1} are almost the same, indicating that the As–Se bonding features are unchanged over the entire x range measured. The shoulder in $S_{\mathrm{SeSe}}(Q)$ at about 15 nm^{-1} becomes prominent, and the height of the first peak decreases with decreasing x. On the other hand, the oscillation beyond 50 nm^{-1} becomes larger, indicating that the number of Se–Se bonds increases.

Here, it should be noted that detailed atomic configurations, particularly intermediate-range order cannot be correctly obtained without including the AXS data. In fact, a recent paper on the structure of As-Se glasses reported the $S_{ij}(Q)$ functions by using a RMC modeling with only total XRD data.[30] However, they highly disagree with the present results in the low Q region up to about 18 nm^{-1}, i.e., the $S_{\mathrm{AsAs}}(Q)$ and $S_{\mathrm{AsSe}}(Q)$ data do not show distinct and systematic prepeaks and the positions of the shoulders in $S_{\mathrm{SeSe}}(Q)$ largely shift towards the shorter Q values forming a small peaks.

Figure 5 shows (a) $g_{\mathrm{AsAs}}(r)$, (b) $g_{\mathrm{AsSe}}(r)$, and (c) $g_{\mathrm{SeSe}}(r)$ of As_xSe_{1-x} glasses obtained from the present RMC fits. On the $g_{\mathrm{AsAs}}(r)$ function of the $As_{0.40}Se_{0.60}$ glass, a large peak is observed at about 0.23 nm with a height of about 2.6, as shown in Fig. 5(a), indicating a large number of As–As homogeneous wrong bonds, which were also reported in the results of the NDIS experiment.[13] With decreasing x, this homopolar peak once decreases in height and becomes broadened in the IP composition range, and again recovers in the floppy region. However, the errors markedly increase in this region owing to the small W^k_{ij} values, and thus,

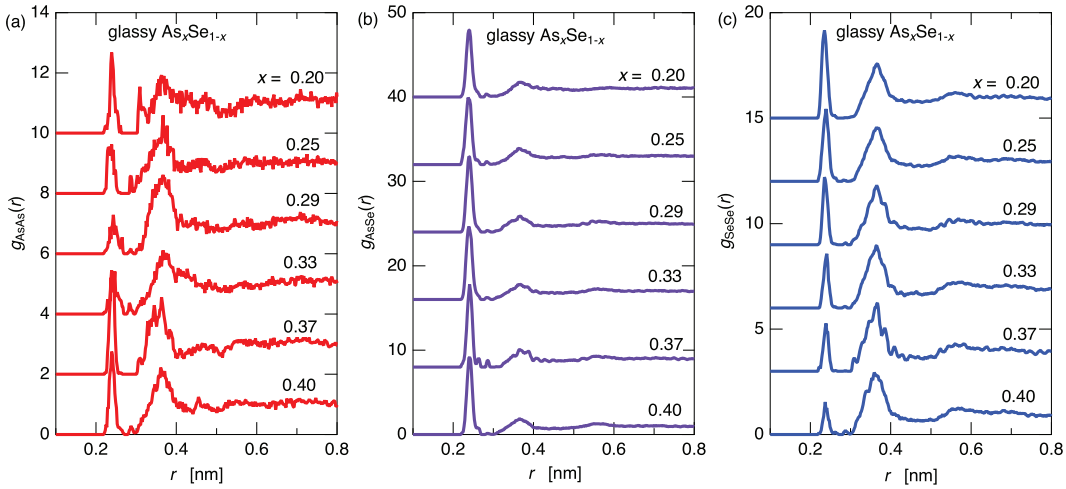

Fig. 5. (a) $g_{AsAs}(r)$, (b) $g_{AsSe}(r)$, and (c) $g_{SeSe}(r)$ of As_xSe_{1-x} glasses obtained by the present RMC modeling. For clarity, the data are displaced upward by 2 for (a), 8 for (b), and 3 for (c). (Color online)

the recovery in the low x region is not a decisive evidence of the prepeak features.

The second peak of $g_{AsAs}(r)$ of the $As_{0.40}Se_{0.60}$ glass is also very high, about 2, representing the correlations between the $AsSe_3$ pyramids with corner- or edge-sharing connections. Since the shoulder at the shorter side of the second peak in not clearly seen, unlike the Ge–Se results,[9,10] the fraction of edge-sharing $AsSe_3$ pyramids would be rather small. With decreasing x, the height of the second peak seems to be almost unchanged, although the $g_{AsAs}(r)$ functions are highly scattered. Beyond the second peak, the statistics are very poor, particularly in the low x region, owing to the small W_{AsAs} values even for the $\Delta_{As}S(Q)$ data, as given in Fig. 2.

For the $g_{AsSe}(r)$ function at $x = 0.40$ shown in Fig. 5(b), a large and sharp first peak is observed at $r \sim 0.240$ nm with a height of about 9. The second peak indicates strong As–Se covalent bonds. The second broad peak is located at about 0.37 nm with a height of about 1.8, exhibiting a Se atom attached to an $AsSe_3$ pyramid, i.e., As–(Se)–Se correlation. Such features in the first and second peaks do not vary with decreasing x. Only a small difference is observed in the third peak detected at about 0.57 nm; it is smeared out with decreasing x.

In Fig. 5(c), when $x = 0.40$, a small peak is found at about 0.237 nm with a height of about 1.5, which again represents the presence of the so-called homopolar *wrong* bonds. With decreasing x, the first Se–Se peak grows gradually and systematically up to a height of about 4 with $x = 0.20$, owing to the extra Se atoms in the glasses. The second maximum of $g_{SeSe}(r)$ when $x = 0.40$ is located at $r \sim 0.36$ nm with a height of about 2.8, originating from Se–(As)–Se correlations inside the $AsSe_3$ pyramid. With decreasing x, the second peak

decreases very gradually in height with a mostly unchanged interatomic length. The change would originate from the decreasing number of pyramids and a wider distribution of the Se–(Se)–Se interatomic distance for the compensating Se chains in the As–Se glasses.

The left panels of Fig. 6 show the 3D atomic configurations obtained by the present RMC modeling at x = (a) 0.40, (b) 0.33, and (c) 0.25. Red tetrahedra indicate the $AsSe_3$ pyramids. The size of each picture in Fig. 6 is about 3.25 nm, being one-half of the RMC simulation boxes. At (a) $x = 0.40$, the $AsSe_3$ pyramids are mainly connected by corner sharing, while a certain number of edge-sharing connections are also observed. As mentioned above, there are certain numbers of homopolar *wrong* bonds. To emphasize them, only the As–As and Se–Se bonds are shown in the right panels of Fig. 6 as solid and dashed lines, respectively, where the atomic configuration is the same as in the left panel. Bonds are defined as lengths below 0.28 nm in the first peak regions in Figs. 5(a) and (c). Although a certain fraction of Se–Se short bonds are formed by large distortions of pyramids, a large number of individual and topologically *wrong* bonds are confirmed in the $As_{0.40}Se_{0.60}$ glass. With decreasing x, the number of Se–Se bonds increases, as expected. On the other hand, a small number of As–As *wrong* bonds remain even at $x = 0.25$ (or at the lowest As fraction of $x = 0.20$, as shown in Fig. 5(a)).

4. Discussion

4.1 Local structures

To discuss partial coordination numbers and bond angles, atomic bonds are again defined as interatomic distances below 0.28 nm, where the first and second peaks in the $g_{ij}(r)$ functions are well separated, as shown in Fig. 5. The partial coordination number, N_{ij}, is defined as the mean number of type j atoms around type i atoms. The previous r_{ij} and N_{ij} results are well compiled by Polidori et al. in Table III of Ref. 13. Table II shows structural parameters of the partial interatomic distance, r_{ij}, and N_{ij} obtained in previous experimental[12–14] and theoretical[31,32] works at selected x values of 0.20, 0.30, and 0.40, as well as the present results at $x = 0.20$, 0.29, and 0.40. The r_{ij} values from the NDIS experiments are not given in the table because the $g_{ij}(r)$ functions were not evaluated owing to the limited number of isotope-enriched samples. The typical values estimated from their analysis are given in parentheses under the r_{AsSe} column.

By comparing the overall features of these parameters, we found a common tendency that the r_{ij} values in the results of AIMD calculations are larger than in those of the experiments by 0.05–0.15 nm. The important advantage of the RMC modeling is that this inverse technique

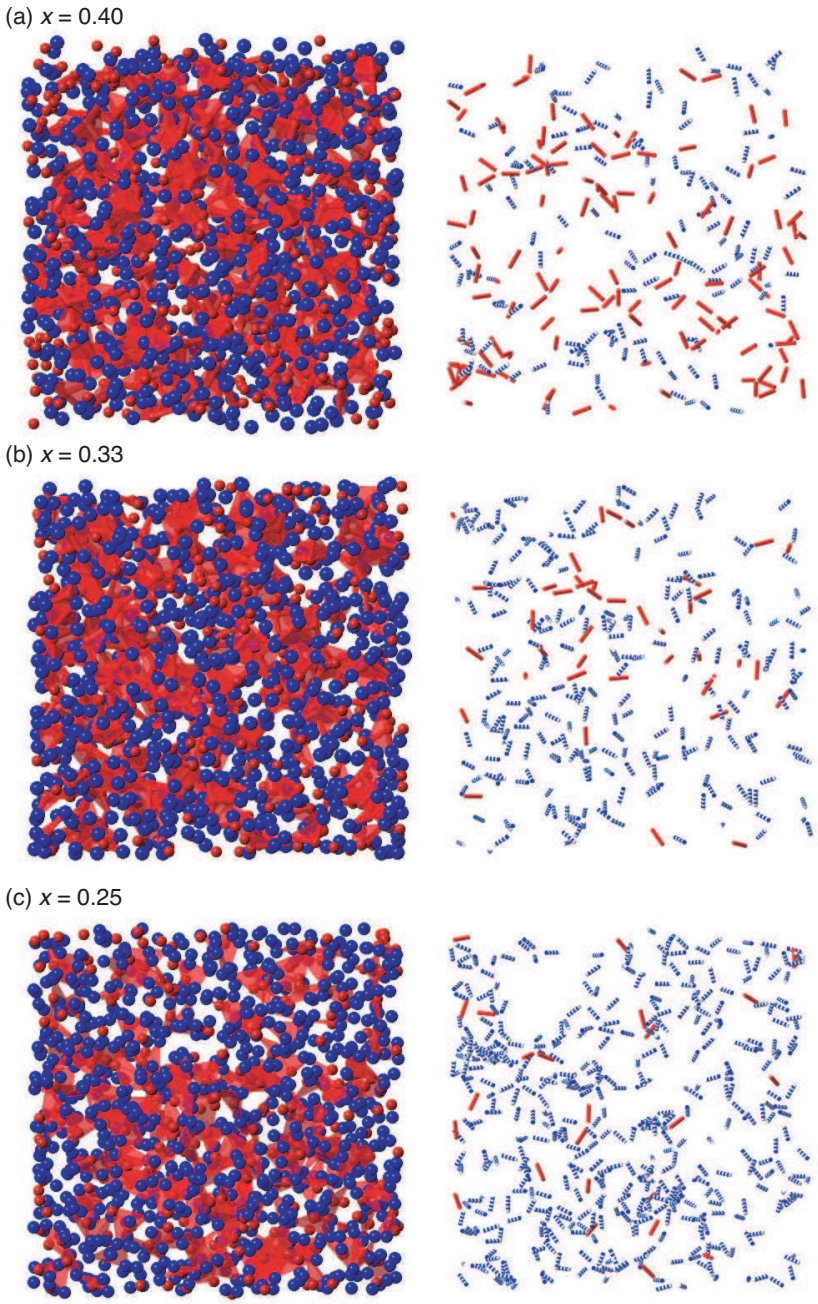

Fig. 6. Atomic configurations of glassy As_xSe_{1-x} obtained by the present RMC modeling at selected x values of (a) 0.40, (b) 0.33, and (c) 0.25. Left panels: $AsSe_3$ pyramidal units. Right panels: As–As and Se–Se homopolar bonds indicated by solid and dashed lines, respectively. (Color online)

can complement the lack of missing data of AXS results in the large Q region, as was clearly given by Waseda et al.[33] The inclusion of ND data over the wide Q range in this study, moreover, made justified our results in the first shell regime. In addition, the total scattering $g(r)$ data on As_2Se_3 glass are dominated by the As–Se heteropolar partial in both XRD and

Table II. r_{ij} (nm), and N_{ij} (atoms) values obtained from present experiments and previous experimental and theoretical works at selected x values.

x	r_{AsAs}	r_{AsSe}	r_{SeSe}	N_{AsAs}	N_{AsSe}	N_{As}	N_{SeAs}	N_{SeSe}	N_{Se}	Ref.
0.40	0.240	0.241	0.238	0.48	2.54	3.02	1.69	0.35	2.04	Present
	0.241	0.237	0.225	0.73	2.53	3.26	1.69	0.32	2.01	AXS[12]
		(0.241)		0.63	2.37	3.00	1.58	0.42	2.00	NDIS[13]
	0.255	0.245	0.237	0.65	2.40	3.05	1.60	0.42	2.02	AIMD[31]
	0.258	0.248	0.242	0.70	2.31	3.01	1.54	0.45	1.99	AIMD[32]
	0.255	0.245	0.240	0.53	2.54	3.07	1.69	0.32	2.01	AIMD[12]
0.30		(0.240)		0.01	2.99	3.00	1.28	0.72	2.00	NDIS[13]
	0.257	0.247	0.239	0.07	2.94	3.01	1.26	0.74	2.00	AIMD[31]
0.29	0.244	0.240	0.237	0.18	2.85	3.03	1.17	0.85	2.02	Present
	0.241	0.235	0.229	0.12	3.57	3.69	1.46	0.54	2.00	AXS[14]
0.20	0.240	0.240	0.235	0.19	2.77	2.96	0.69	1.35	2.04	Present
	0.259	0.247	0.239	0.05	2.96	3.01	0.74	1.27	2.01	AIMD[31]

ND results, and the obtained first peak position has been at about 0.241 nm consistently since the 1970s[29,34] to now.[13,35] Furthermore, the r_{SeSe} value should approach the interatomic distance of Se glass of about 0.234 nm[29,36] with decreasing x. Therefore, the experimental r_{ij} values are correct and the theoretical ones have systematic deviations to larger values.

Other large differences are seen in the coordination numbers obtained from previous AXS experiments.[12,14] In particular, the N_{As} values are much larger than the $8 - N$ rule of three. There may be two reasons why the results are different. First, we used the experimentally obtained anomalous terms, f' and f'', for the atomic form factors f, as shown in Fig. 1 and Table I, which improved the qualities of the $\Delta_k S(Q)$ functions and the RMC analysis, rather than the theoretical values in the previous papers.[12,14] Second, the $S_{\mathrm{N}}(Q)$ and $g_{\mathrm{N}}(r)$ data were included in the present RMC analysis, as shown in Figs. 3(d) and (e). As mentioned above, owing to a wide Q range measured by ND, the validity of the information on the first nearest neighbors is highly improved compared with the results of the RMC analysis without ND data. By comparing with the NDIS results by Polidori et al.,[13] the N_{AsAs} value of 0.01 at $x = 0.30$ is much smaller than the present value of o.18 at $x = 0.29$. Such a discrepancy may result from the fact that no good As isotopes exists in the NDIS measurement. The existence of $\Delta_{\mathrm{As}} S(Q)$ data in our AXS measurements may give correct $S_{\mathrm{AsAs}}(Q)$, $g_{\mathrm{AsAs}}(r)$, and N_{AsAs} values.

Figure 7 shows the x dependence of the N_{ij} values obtained from the present RMC anal-

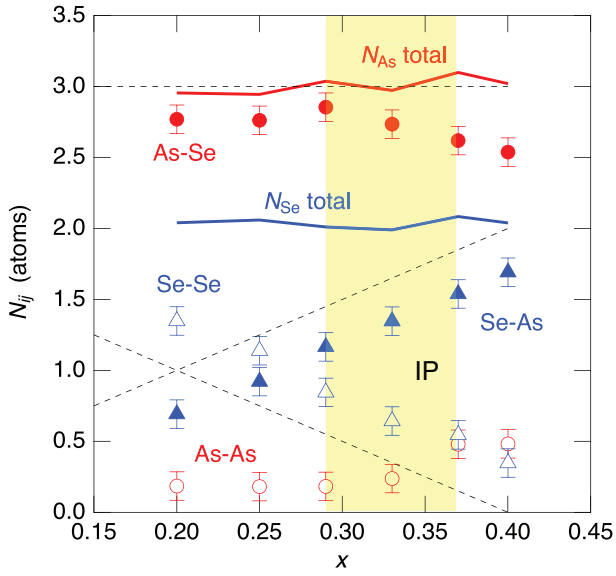

Fig. 7. Averaged partial coordination numbers N_{ij}. Solid curves represent total coordination numbers around As (upper) and Se (lower) atoms. Dashed lines indicate the ideal N_{ij} values assuming the chemically ordered continuous-random-network model.[37] (Color online)

ysis. For the annotations in the figure, As–As and As–Se indicate N_{ij} values for neighboring As and Se atoms around As, and similarly, those around Se are given as Se–As and Se–Se. Dashed lines indicate the ideal N_{ij} values predicted by Zachariasen using a chemically ordered continuous-random-network model.[37] The solid curves represent the total coordination numbers around As and Se (N_{As} and N_{Se}), which are almost 3 and 2, respectively, in the $0.20 \leq x \leq 0.40$ range. This result indicates that the $8 - N$ bonding rule is applicable to As_xSe_{1-x} glasses for all the concentrations measured.

At $x = 0.40$, the majority of the As and Se atoms are surrounded by three Se and two As atoms, respectively. The average numbers of homopolar As–As and Se–Se *wrong* bonds are 0.48 ± 0.10 and 0.35 ± 0.10, respectively. The N_{AsAs} value of 0.48 is slightly smaller than others as shown in Table II, but acceptable within the range of errors of the present and previous studies. The N_{AsAs} value is in agreement with those obtained from other experimental and theoretical works. As mentioned above, $N_{As} \sim 3.0$ and $N_{Se} \sim 2.0$ are concluded from the results of the present experiments, which contradicts the previous AXS result of a breaking down of the $8-N$ rule around As by Hosokawa et al.[12] and the prediction of an additional As–Se double bond on the basis of the mean-field theory.[11] Owing to the improvements of the present experiments and analyses by using the experimental f' and f'' values and including ND data, the conclusion in the previous paper regarding As_2Se_3 glass, i.e., the breakdown of

the $8 - N$ rule, is doubtful.

With decreasing x, N_{SeAs} decreases and N_{SeSe} increases, which is mostly in line with the results of the chemically ordered continuous-random-network model[37] shown by the dashed lines in Fig. 7, except for the presence of homopolar *wrong* bonds. Note that N_{AsAs} largely decreases from about 0.5 to about 0.2 when crossing the IP concentration range indicated in yellow color in Fig. 7. This phenomenon would be reasonable because the As–As *wrong* bonds reflect the stressed-rigid nature of the As_xSe_{1-x} glasses at $x > 0.36$, and the stress in the glasses is released in the IP region, as was found in the Ge–Se glasses.[10] In the floppy region of $x < 0.26$, there are a certain number of As–As bonds, i.e., the *wrong* bonds intrinsically remain even in the flexible As–Se networks.

Figure 8 shows the (a) As–Se–As and (b) Se–As–Se bond angle distributions of As_xSe_{1-x} glasses as a function of $\cos\theta$. The θ values are indicated at the top of the figures. At $x = 0.40$, the As–Se–As and Se–As–Se distributions have broad peaks centered at about 97° and 100°, respectively. The As–Se–As and Se–As–Se bond angles of crystalline As_2Se_3 with a monoclinic space group have three different values in the ranges of 85.6–101.5° and 90.6–104.3°,[38] respectively, and the glass phase has slightly larger angles. The bond angle distributions at $x = 0.40$ were examined experimentally with the usual combination of XRD, ND, and RMC analysis by Fábián et al.,[35] and the peak positions of 97 ± 2° and 99 ± 2° were obtained for the As–Se–As and Se–As–Se configurations, respectively, in good agreement with the present results although they did not utilize the AXS or NDIS data of greater element sensitivity.

To our knowledge, there have been two AIMD studies of the bond angle distributions of As_2Se_3 glass,[31,39] and both studies indicated broad distributions around either As or Se centered at about 100°. A specific result was given for the As–Se–As bond angle distributions by Bauchy et al.[31] where there is an additional shoulder at about 90°. They did not identify the origin of the shoulder, and it is too large to be composed of edge-sharing $AsSe_3$ pyramids, in contrast to those of $GeSe_4$ tetrahedra in $GeSe_2$ glass.[10]

With decreasing x, the As–Se–As distributions become rather broad and scattered owing to the decrease in the number of the pyramid connections with only one Se atom (Se_1), as shown later. The As–Se–As bond angle distributions shown in Fig. 8(a) do not seem to change systematically from the broad peak centered at about 97° at $x = 0.40$. However, it is clear that the broad peak is suddenly smeared out below $x = 0.25$, which may be related to that the glass system enters the floppy regime. The Se–As–Se distributions remain mostly unchanged, whereby the local atomic configurations of $AsSe_3$ pyramids do not change with x. Only Bauchy et al.[31] discussed the x dependence of the bond angle distributions by obtaining

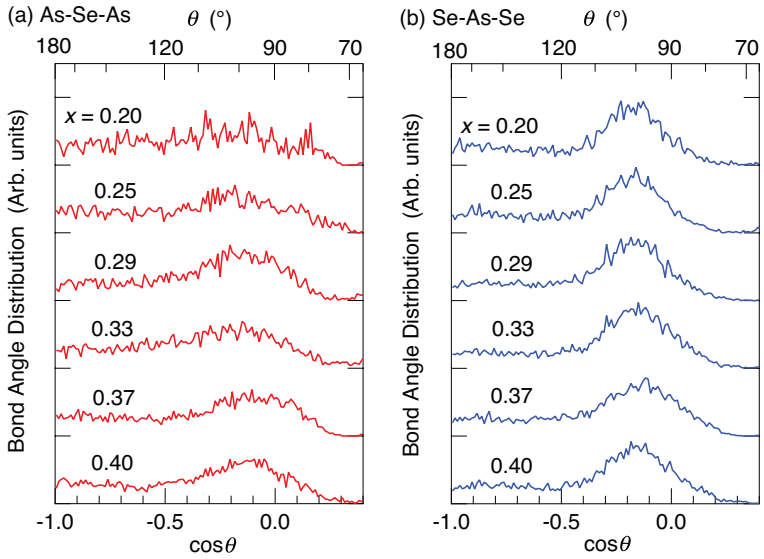

Fig. 8. Distributions of (a) As–Se–As and (b) Se–As–Se bond angles. Curves are displaced upward for clarity. (Color online)

four types of bond angle (Se–Se–As and Se–Se–Se in addition to the above), and rather complex x dependences were reported. In addition, they obtained the x dependence of the average dihedral angle and the standard deviation, which indicate rather characteristic features in the IP concentration region. On the other hand, the experimentally obtained results in the present work show simple and gradual x variations, and cannot compare with the above theoretical predictions.

4.2 Intermediate-range order

A prepeak in the $S(Q)$ spectra in covalent glasses suggests the existence of intermediate-range order (IRO) in the atomic configurations of glasses. Large changes were observed in the total $S(Q)$ of Ge_xSe_{1-x} glasses,[9,10,40] where with decreasing x, the position largely shifts towards larger Q values and the height rapidly decreases, as shown in Figs. 2(c) and (d) of Ref. 10 for the XRD and ND data, respectively. By separating them into the partial $S_{ij}(Q)$s, it was found that with decreasing x, the prepeaks in the Ge–Ge and Ge–Se partials show slight increases in position, while the shoulder position in $S_{\mathrm{SeSe}}(Q)$ rapidly decreases. The prepeak height in $S_{\mathrm{GeGe}}(Q)$ rapidly decreases in the IP concentration range of $0.26 \geq x \geq 0.20$. These partial behaviors in the prepeak/shoulder induce the interesting changes in the prepeak of the total $S(Q)$ of Ge_xSe_{1-x} glasses.

In the present As_xSe_{1-x} case, the x dependence of the prepeak in total $S(Q)$ is very small, as shown in Figs. 3(c) and (d), with only peak heights decreasing with decreasing x. Figure

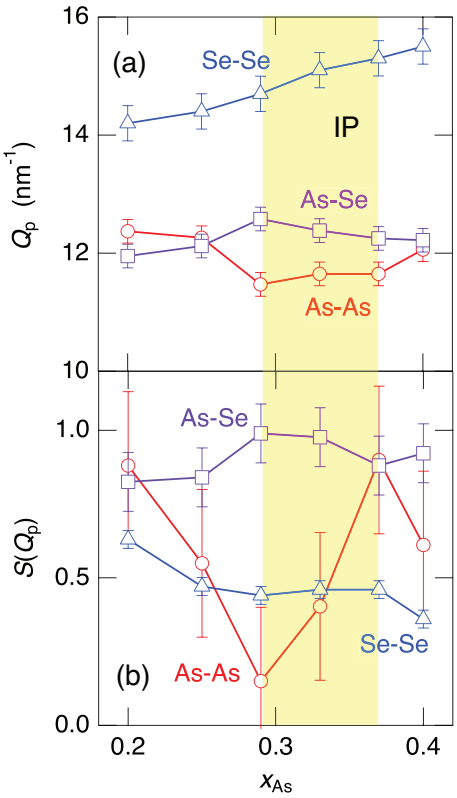

Fig. 9. (a) Q_p and (b) $S_{ij}(Q_p)$ in the As–As (◯), As–Se (□), and Se–Se (△) partials of $S_{ij}(Q)$s. (Color online)

9(a) shows the x dependence of the prepeak/shoulder positions, Q_p, in the As–As, As–Se, and Se–Se partials of $S_{ij}(Q)$ indicated by circles, squares, and triangles, respectively, which are obtained from Fig. 4. The peak positions of the As–As and As–Se correlations show mostly the same values of about 12 nm^{-1}, and that of Se–Se gradually decreases with decreasing x. In the hatched IP concentration region, the decreasing rate is slightly higher, but not so prominent as that of the Ge–Se glasses shown in Fig. 7(a) of Ref. 10.

Figure 9(b) shows the heights of the prepeaks for the partials, $S_{ij}(Q_p)$. The prepeak heights for As–Se are almost a constant value of about 0.9, and those of Se–Se show a gradual increase from 0.4 to 0.6 with decreasing x. On the other hand, those of As–As have a rather scattered x dependence owing to the small W_{AsAs} values, as shown in Fig. 2. If anything, a decrease is observed in the IP concentration region, while it is not clear when compared with the Ge–Ge prepeak height in Ge_xSe_{1-x} glasses in the IP region. The x dependence in the features of prepeaks in the As–Se glasses have been taken up only for total $S(Q)$ functions,[41,42] and the relationship to the stiffness transition has not been discussed clearly. Golovchak et al. reported that the prepeak width increases at about $x = 0.3$ in both the XRD and ND data.[42] On the other hand, the present data cannot clarify such a broadening as anything other than

Table III. x dependence of the fractions of corner-, edge-, and face-sharing connections between the $AsSe_3$ pyramids.

x	F_{corner} (%)	F_{edge} (%)	F_{face} (%)
0.40	92.5	7.4	0.1
0.37	91.8	8.0	0.2
0.33	90.8	8.6	0.6
0.29	92.3	7.0	0.8
0.25	92.4	7.5	0.1
0.20	92.4	7.5	0.1

experimental error.

Next, we discuss the connections of the $AsSe_3$ pyramids. In crystalline monoclinic As_2Se_3, the pyramids are connected with each other by fully corner-sharing configurations.[38] Table III shows the x dependence of the corner-, edge-, and face-sharing connections when two As atoms approach each other as second neighbors by sharing a Se atom. As for the As_2Se_3 glass at $x = 0.40$, only about 7.5% of pyramids are connected accidentally by edge sharing, and corner sharing dominates the pyramid connections. This value is much smaller than the edge-sharing fractions of $GeSe_4$ tetrahedra (20–25%) in the stressed-rigid region of the Ge–Se glasses, as shown in Fig. 11(b) of Ref. 10. The face-sharing connection is negligible. With decreasing x, all fractions remain basically unchanged, which is unlike the Ge–Se glass case, where the edge-sharing fraction rapidly decreases, as shown in Fig. 11(b) of Ref. 10. These differences would be due to the fact that the $AsSe_3$ pyramid clusters do not include the stresses caused by the overconstraint of the averaged coordination numbers.

Then, we discuss the connections between two pyramids. As mentioned above, the majority of the connections between the $AsSe_3$ pyramids in the As_2Se_3 glass are corner sharing, and there are a small fraction of edge-sharing connections. For both connections, the As atoms share only one Se atom between them; this was referred to as the S_1 connection in the previous discussion. At the As_2Se_3 composition, the glass system is considered to be in the stressed-rigid region.[11] Figure 10 shows the x dependence of the fraction of the number of Se atoms belonging to Se_n chains between two As atoms, i.e., the fraction of Se atoms intervening between the As atoms.

At $x = 0.40$, about 72% of Se atoms are connected with two As atoms by corner-, edge- or face-sharing connections (Se_1). About 18% of Se atoms form the As–Se–Se–As connections (Se_2). The remaining 10% of Se atoms are located in longer Se chains between two As atoms.

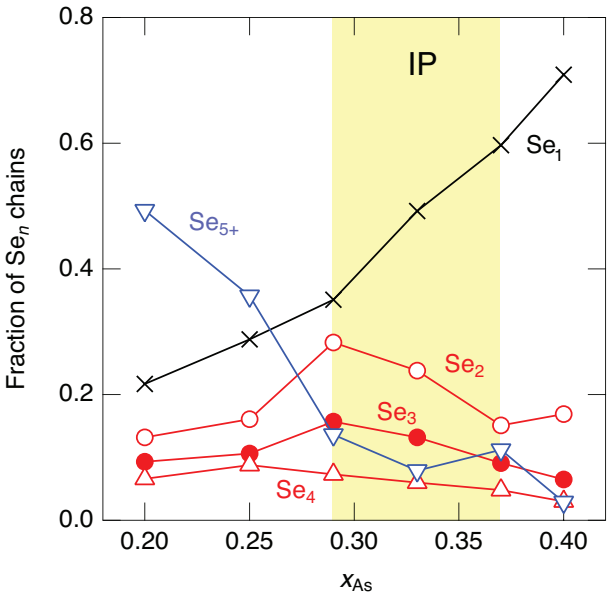

Fig. 10. Fraction of the number of Se atoms belonging to Se_n chains. The yellow region represents the IP concentration region. (Color online)

With decreasing x, the fraction of S_1 connections gradually decreases owing to the increase in the numbers of Se atoms in the glasses. The fraction of Se_2 connections increases until the end of the IP region at $x = 0.29$, and then starts to decrease rapidly. The S_3 connections exhibit a similar x dependence to the Se_2 connections with a smaller fraction of about 3/5. On the other hand, the fraction of Se atoms belonging to longer chains of more than five Se atoms rapidly increases in the floppy region of $x < 0.29$.

A similar analysis was carried out on Ge_xSe_{1-x} glasses, and the following results were obtained in relation to the stiffness transition shown in Fig. 12 of Ref. 10. Firstly, the fraction of Se_1 atoms exhibits a dip in the IP region in Ref. 10, while the present result does not. Secondly, the fraction of Se_2 connections slightly decreases in this region, which contradicts the present result. Thirdly, the fraction of Se_{4+} connections (Se atoms belonging to chains with more than 4 atoms) exceeds that of S_1 connections at the central composition of the IP region, whereas the S_1 connections are dominant there in the present As–Se glasses, and the rapid increase in S_{4+} ($= S_4 + S_{5+}$) starts at the end of the IP region. In the previous paper on the Ge–Se glasses, it was discussed that these behaviors of the connections of $GeSe_4$ tetrahedra originate from a large configurational stress in the Se_2 connections and a relevant phase separation tendency between the S_1 and S_{4+} chain connections. In the present As–Se glasses, on the other hand, such presence of stresses is hardly expected because $AsSe_3$ pyramids have good constraints to form glasses in the sense of rigidity percolation theory and

do not form a specified configuration nearby. Accordingly, the differences in the pyramidal connections may be related to the anisotropic pyramidal atomic configurations around the As atoms in the As-Se glasses in contrast to the isotropic tetrahedral ones around the Ge atoms in the Ge-Se glasses.

5. Conclusions

AXS, XRD, and ND experiments were carried out on As_xSe_{1-x} chalcogenide glasses and the results were analyzed by RMC modeling to obtain the partial atomic structural information in $S_{ij}(Q)$s, $g_{ij}(r)$s, and 3D atomic configurations and to find the relationship between them and the stiffness transition. By using the experimentally obtained anomalous terms for the atomic form factors and including the ND data for RMC analysis, the quality of the partial structural results was highly improved, particularly for the coordination numbers. The $S_{ij}(Q)$ and $g_{ij}(r)$ functions seem to gradually change with x; however, an important change is detected, i.e., a rapid decrease of As–As wrong bonds is visualized in the IP region, as in the Ge–Se glasses.[10] However, the other anomalies found in the Ge–Se glasses, such as a rapid decrease in the pre-shoulder position in $S_{\mathrm{SeSe}}(Q)$, a rapid decrease in the number of edge-sharing connections, and an exclusion tendency of the connections between the As(Ge) atoms sharing two Se atoms, were not clearly observed. These differences may be due to the fact that the $AsSe_3$ pyramids in the As–Se glass do not have any structural stress in contrast to the $GeSe_4$ tetrahedra in the Ge–Se glasses.

Finally, we note that the qualities of $S_{\mathrm{AsAs}}(Q)$ and $g_{\mathrm{AsAs}}(r)$ are not sufficient probably because of the small W_{AsAs} values even in the $\Delta_{\mathrm{As}}S(Q)$ spectra of the AXS data. In particular, the prepeaks seem not to change systematically in height with x and are not in good agreement with the existing AIMD data.[31] A possible way of improving the data quality with partial information is to include the NDIS data, as shown in Ref. 13, in the RMC analysis; this is now being planned.

Another way to improve the structural information is to ameliorate the statistics of the AXS data by increasing the incident X-ray flux. Since the beamline at the ESRF used for the present study is a bending magnet one, it is possible to replace it with an undulator insertion device for the X-ray source. At the SPring-8, new AXS equipments have been developed at previously BL13XU and currently BL47XU, and an intenser X-ray beam (about two orders of magnitude) and a better energy resolution using a LiF analyzer crystal (about 30 eV at 10 keV[43]) were achieved.[44,45] In fact, much reasonable results in the pre- and first peak region of $\Delta_{\mathrm{Ga}}S(Q)$ were obtained on a $Ga_2Ge_3Se_9$ glass at the SPring-8[46] compared with that

measured at the ESRF,[47] and the similar improvements is highly expected for the present As-Se glasses.

Acknowledgment

The AXS experiments were performed at BM02 of the ESRF (No. HS1860) and at BL15 of the Saga-LS (Nos. 1802007A and 2005048F). The supporting AXS experiments were carried out at BL13XU (Nos. 2021A1181 and 2021B1110), and BL47XU (No. 2022A1306). The ND measurements were carried at BL21 of MLF in the J-PARC (No. 2017B0047). SH acknowledges the Japanese Society for Promotion of Science (JSPS) for Grant-in-Aids for Transformative Research Areas (A) 'Hyper-Ordered Structures Science' (Nos. 21H05569 and 23H04117) and for Scientific Research (C) (No. 22K12662), and Japan Science and Technology Agency (JST) for CREST (No. JPMJCR1861) for financial supports.

References

1) J. C. Phillips, J. Non-Cryst. Solids **34**, 153 (1979).
2) M. F. Thorpe, J. Non-Cryst. Solids **57**, 355 (1983).
3) S. S. Yun, H. Li, R. L. Cappelletti, R. N. Enzweiler, and P. Boolchand, Phys. Rev. B **39**, 8702 (1989).
4) Y. Wang, M. Nakamura, O. Matsuda, and K. Murase, Physica B **263–264**, 313 (1999).
5) M. Tatsumisago, B. L. Halfpap, J. L. Green, S. M. Lindsay, and C. A. Angell, Phys. Rev. Lett. **64**, 1549 (1990).
6) R. Böhmer and C. A. Angell, Phys. Rev. B **45**, 10091 (1992).
7) X. Feng, W. J. Bresser, and P. Boolchand, Phys. Rev. Lett. **78**, 4422 (1997).
8) P. Boolchand, X. Feng, and W. J. Bresser, J. Non-Cryst. Solids **293–295**, 348 (2001).
9) S. Hosokawa, I. Oh, M. Sakurai, W.-C. Pilgrim, N. Boudet, J.-F. Bérar, and S. Kohara, Phys. Rev. B **84**, 014201 (2011).
10) S. Hosokawa, Y. Kawakita, L. Pusztai, K. Ikeda, and T. Otomo, J. Phys. Soc. Jpn. **90**, 024601 (2021).
11) D. G. Georgiev, P. Boolchand, and M. Micoulaut, Phys. Rev. B **62**, R9228 (2000).
12) S. Hosokawa, A. Koura, J.-F. Bérar, W.-C. Pilgrim, S. Kohara, and F. Shimojo, Europhys. Lett. **102**, 66008 (2013).
13) A. Polidori, A. Zeidler, snd P. S. Salmon, J. Chem. Phys. **153**, 154507 (2020).
14) S. Hosokawa, W.-C. Pilgrim, J.-F. Bérar, and P. Boolchand, J. Non-Cryst. Solids **431**, 31 (2016).
15) J. R. Stellhorn, S. Hosokawa, and E. Magome, AIP Conf. Proc. **2054**, 050012 (2019).
16) S. Hosokawa, J. R. Stellhorn, W.-C. Pilgrim, and J.-F. Bérar, Z. Phys. Chem. **230**, 313 (2016).
17) S. Sasaki, *KEK Report 88-14*, Nat. Lab. High Energy Phys., Tsukuba, Japan, 1989, pp. 1–136.
18) I. Petri, P. S. Salmon, and H. E. Fischer, Phys. Rev. Lett. **84**, 2413 (2000).
19) C. H. MacGillavry and G. D. Rieck, (ed.), *International Tables for X-ray Crystallography, 2nd ed.*, Kynoch Press, Birmingham, UK, 1968.
20) See `https://j-parc.jp/researcher/MatLife/en/instrumentation/ns_spec.html#bl21`.

21) H. H. Paalman and C. J. Pings, J. Appl. Phys. **33**, 2635 (1962).

22) I. A. Blech and B. L. Averbach, Phys. Rev. **137**, A1113 (1965).

23) V. F. Sears, Neutron News **3**, 26 (1992).

24) NOVA project, *Analysis of Ordered/Disordered Structure in Hydrides with Total Scattering Technique* (2015). See `http://research.kek.jp/group/hydrogen/analysis.html`.

25) R. L. McGreevy and L. Pusztai, Mol. Simul. **1**, 359 (1988).

26) R. L. McGreevy and M. A. Howe, Annu. Rev. Mater. Sci. **22**, 217 (1992).

27) C. T. Hach, K. Cerqua-Richardson, J. R. Varner, and W. C. LaCourse, J. Non-Cryst. Solids **209**, 159 (1997).

28) O. Gereben, P. Jóvári, L. Temleitner, and L. Pusztai, J. Optoelectron. Adv. Mater. **9**, 3021 (2007).

29) A. L. Renninger and B. L. Averbach, Phys. Rev. B **8**, 1507 (1973).

30) A. F. Elhady, M. Dongol, E. Toliba, and M. S. Ebied, Mater. Today Commun. **37**, 106927 (2023).

31) M. Bauchy, A. Kachmar, and M. Micoulaut, J. Chem. Phys. **141**, 194506 (2014).

32) J. Li and D. A. Drabold, Phys. Rev. B **61**, 11998 (2000).

33) Y. Waseda, S. Kang, K. Sugiyama, M. Kimura, and M. Saito, J. Phys.: Condens. Matter **12**, A195 (2000).

34) Y. Sagara, O. Uemura, S. Okuyama, and T. Satow, Phys. Status Solidi A **31**, K33 (1975).

35) M. Fábián, E. Sváb, V. Pamukchieva, A. Szekeres, P. Petrik, S. Vogel, and U. Ruett, J. Non-Cryst. Solids **358**, 860 (2012).

36) A. Zeidler, P. S. Salmon, D. A. J. Whittaker, K. J. Pizzey, and A. C. Hannon, Front. Mater. **4**, 32 (2017). The numerical value is given in Ref. 13.

37) W. H. Zachariasen, J. Am. Chem. Soc. **54**, 3841 (1932).

38) A. C. Stergiou and P. J. Rentzeperis, Z. Kristallogr. **173**, 185 (1985).

39) J. Li and D. A. Drabold, Phys. Rev. B **64**, 104206 (2001).

40) Y. Wang, E. Ohata, S. Hosokawa, M. Sakurai, and E. Matsubara, J. Non-Cryst. Solids **337**, 54 (2004).

41) E. Bychkov, C. J. Benmore, and D. L. Price, Phys. Rev. B **72**, 172107 (2005).

42) R. Golovchak, P. Lucas, J. Oelgoetz, A. Kovalskiy, J. York-Winegar, Ch. Saiyasombat, O. Shpotyuk, M. Feygenson, J. Neuefeind, and H. Jain, Mater. Chem. Phys. **153**, 432 (2015).

43) S. Hosokawa, K. Kobayashi, A. Koura, F. Shimojo, Y. Tezuka, J. Adachi, Y. Onodera, S. Kohara, H. Tajiri, A. Chokkalingam, and T. Wakihara, Microporous Mesoporous Mater. **359**, 112662 (2023).

44) S. Kohara, H. Tajiri, C. H. Song, K. Ohara, L. Temleitner, K. Sugimito, A. Fujiwara, L. Pusztai, T. Usuki, S. Hosokawa, Y. Benino, N. Kitamura, and K. Fukumi, J. Phys. Conf. Ser. **502**, 012014 (2014).

45) S. Kohara, K. Ohara, H. Tajiri, C. H. Song, O. Sakata, T. Usuki, Y. Benino, A. Mizuno, A. Masuno, J. T. Okada, T. Ishikawa, and S. Hosokawa, Z. Phys. Chem. **230**, 339 (2016).

46) S. Hosokawa, J. R. Stellhorn, Y. Onodera, S. Kohara, H. Tajiri, E. Magome, L. Pusztai, K. Ikeda, T. Otomo, M. Krbal, and T. Wagner, JPS Conf. Proc. **33**, 011069 (2021).

47) B. D. Klee, J. R. Stellhorn, M. Krbal, N. Boudet, G. Chahine, N. Blanc, W.-C. Pilgrim, T. Wagner, and S. Hosokawa, Chalc. Lett. **15**, 1 (2018).